The Study of Fragrance Encapsulation Using Zeolite

Natnicha Kongyang, *Sukanya* Sudmee, *Rapeeporn* Wannarat, and *Sukanya* Thepwatee

Department of Industrial Chemistry, Faculty of Applied Science, King Mongkut's University of Technology North Bangkok, Wong Sawang, Bang Sue, 10800 Bangkok, Thailand

Abstract. Aroma is a key component in food, cosmetics, and consumer products, significantly influencing human perception and satisfaction. However, most fragrances are volatile and susceptible to degradation upon exposure to air, heat, and light, reducing product quality and shelf life. Therefore, the development of efficient encapsulation systems for fragrance retention and controlled release is essential. This study investigates the use of zeolites—nanoporous materials with high specific surface areas and excellent adsorption capabilities—as encapsulation carriers for three commonly used cosmetic fragrances: D-limonene (DL), benzyl acetate (BA), and geraniol (GE), which vary in molecular size. The encapsulation efficiency (%EE) and loading efficiency (%LE) of each fragrance were evaluated and compared. The effect of incorporating Tween 80 (T80), a nonionic surfactant, into the system was also examined. Fragrance content and stability were analyzed using thermogravimetric analysis (TGA) one day after preparation and after 30 days of storage at ambient temperature. Results indicated that the presence of T80 helped stabilize %EE and %LE across different fragrance types, whereas in the absence of T80, encapsulation performance appeared more dependent on fragrance molecular characteristics. Additionally, retention studies revealed that systems containing T80 exhibited improved fragrance retention, particularly for low molecular weight, highly volatile compounds. These findings suggest that T80 may modulate the interaction between fragrance molecules and zeolite surfaces, improving both initial loading and long-term retention. This knowledge supports the development of more effective fragrance delivery systems for applications requiring sustained aroma release.

1 Introduction

Fragrance plays a vital role in consumer perception and product appeal in food, cosmetics, and household items [1-3]. However, due to the high volatility of most fragrance compounds, their aroma is rapidly lost when exposed to the atmosphere, leading to diminished product quality and a reduced lifespan of the fragrance. Encapsulation technology offers an effective strategy to protect fragrances, control their release, and prolong their sensory impact [4]. Zeolites have attracted interest as encapsulation materials because of their nanoporous architecture, large surface area, strong adsorption capabilities, and compatibility with biological systems, making them ideal carriers for volatile organic compounds [5-7]. Their pore size and surface characteristics are critical for the physical entrapment and selective adsorption of fragrance compounds.

In addition, formulation additives such as surfactants can significantly influence encapsulation performance. Tween 80 (T80), a non-ionic surfactant, is commonly used to stabilize emulsions and improve the dispersion of active compounds [8, 9]. In the context of fragrance encapsulation, T80 may affect the interaction between zeolites and fragrance molecules by modulating surface affinity or altering molecular mobility [10]. However, to the best of our knowledge, no previous studies have specifically investigated this effect.

Therefore, this study aims to develop an effective fragrance encapsulation system using natural zeolite in combination with T80 as the carrier and retention-enhancing agent for three model fragrance compounds: D-limonene (DL), benzyl acetate (BA), and geraniol (GE). These fragrances were selected based on their structural diversity, molecular weight, and common use in cosmetic applications [11-13]. Encapsulation was performed with and without the addition of 1% (w/v) T80 to assess its role in modifying fragrance–zeolite interactions. Encapsulation performance was evaluated through loading efficiency (%LE) and encapsulation efficiency (%EE), followed by stability assessment using thermogravimetric analysis (TGA) after 30 days of storage at ambient temperature. The effects of molecular characteristics and T80 on fragrance retention were compared. This work explores how molecular size, volatility, and surfactant-assisted modifications influence the encapsulation and long-term stability of fragrances in zeolite-based systems, contributing to the development of more efficient delivery platforms for products requiring prolonged aroma release.

2 Materials and Methods

2.1 Materials

Natural cosmetic-grade zeolite was purchased from Tropicalife Co., Ltd. (Thailand). Ethanol was obtained from the Liquor Distillery Organization (Thailand). Cosmetic-grade D-limonene (DL, 95.0%), geraniol (GE, 95.0%), and benzyl acetate (BA, 99.0%) were supplied by Chanjao Longevity Co., Ltd. (Thailand). Cosmetic-grade Tween 80 (T80, 90.0%) was provided by S. Tong Chemicals Co., Ltd. (Thailand). All chemicals were used as received without further purification.

2.2 Encapsulation of fragrance

The fragrance encapsulation procedure was based on methods described in earlier studies [4, 10]. Zeolite was pre-treated by drying in a vacuum oven (BINDER GmbH, Germany) at 80°C for 2 h. After pretreatment, 1.0 g of zeolite was dispersed into a solution of 15 mL ethanol and 0.200 g T80, with gentle stirring to ensure homogeneity. Then, 5 mmol of a selected fragrance compound was added to the mixture, which was continuously stirred at 60 °C using a magnetic stirrer set to 700 rpm until a dry, powder-like product was formed. The resulting fragrance-loaded zeolite powder was subsequently dried in a hot air oven (Model T6120, Heraeus Instruments, Germany) at 60°C for 2 h.

2.3 Characterization

2.3.1 UV-vis analysis of fragrance compounds

UV–vis absorption spectra of the fragrance molecules were recorded using a SPECORD 210 PLUS UV–vis spectrophotometer (Analytik Jena, Germany). Ethanol was used as both the solvent and blank in the spectral range of 190–1000 nm, using a quartz cuvette.

2.3.2 SEM

The surface morphology of the zeolite was examined using a scanning electron microscope (SEM, FEI QUANTA 450) at 5000× magnification. Prior to imaging, samples were dried in a vacuum oven at 80°C for 3 h, mounted on SEM stubs using carbon adhesive tape, coated with platinum (Pt) at 10 kV and 30 mA, and then directly introduced into the chamber for imaging.

2.3.3 X-ray diffraction

The crystalline structure of zeolite samples were analyzed using X-ray diffraction (XRD) using a D2 PHASER diffractometer (Bruker, Germany) equipped with Cu-Kβ radiation (λ = 1.3923 Å), operating at 40 kV and 30 mA. Scans were recorded over a 2θ range of 1° to 80°, with a step size of 0.02° and a scan speed of 1.20 °/min.

2.3.4 N_2 adsorption-desorption

Prior to nitrogen adsorption–desorption analysis, the zeolite sample was first heated in a vacuum oven at 80 °C for 3 h, followed by pretreatment under a nitrogen gas flow (50 mL/min) at 250°C for 4 h. The adsorption–desorption isotherm, specific surface area, pore size, and pore volume of the zeolite were determined via N_2 adsorption–desorption analysis conducted at -196°C using a BELSORP-mini instrument (BEL, Japan). The specific surface area was evaluated using the Brunauer–Emmett–Teller (BET) equation, while the pore size and pore volume were calculated using the Barrett–Joyner–Halenda (BJH) method [14].

2.3.5 Color measurement

Color analysis of the zeolite samples before and after fragrance loading was performed using the CIELAB color model and reported in the Lab color space using an eXact™ XP spectrophotometer (X-Rite, USA). In this model, the L value represents lightness, ranging from 0 (black) to 100 (white). The a* coordinate reflects the green-to-red spectrum, where negative values indicate green and positive values indicate red. The b* coordinate corresponds to the blue-to-yellow range, with negative values representing blue and positive values indicating yellow. The overall color change (ΔE) between the fragrance-loaded and natural zeolite samples was calculated using Equation (1) [15]:

$$\Delta E = \sqrt{\Delta L^2 + \Delta a^2 + \Delta b^2} \quad (1)$$

2.3.6 FTIR

Functional groups present in the starch samples were characterized using a FT-IR spectrometer (PerkinElmer Spectrum 100, USA). Each sample was blended with potassium bromide (KBr) and compressed into translucent pellets using a manual hydraulic press at a pressure of 5 N/m^2 for 3 min. Spectra were recorded in the range of 450–4000 cm^{-1} at a resolution of 4 cm^{-1}, with eight scans per sample.

2.3.7 TGA

Thermogravimetric analysis (TGA) was performed to determine the fragrance loading efficiency (%LE) and encapsulation efficiency (%EE). The analyzed samples included: zeolite, zeolite loaded with a fragrance molecule, and zeolite loaded with a fragrance molecule and Tween 80 (T80). Each sample (10 mg) was analyzed using a TGA/DSC 3+ thermogravimetric analyzer (Mettler-Toledo Ltd., Thailand) under an air atmosphere at a flow rate of 50 cm^3/min. The temperature was ramped from 50 to 700°C at a heating rate of 10 °C/min. The %LE and %EE were calculated using Equations (2) and (3), respectively:

$$\%LE = \frac{W_F}{W_{ZL}} \times 100 \quad (2)$$

$$\%EE = \frac{W_F}{W_{F0}} \times 100 \quad (3)$$

where W_F is the weight of encapsulated fragrance, W_Z is the weight of zeolite, and W_{F0} is the initial weight of the fragrance loaded.

2.4 Fragrance retention

Fragrance retention was evaluated by storing the encapsulated fragrance samples in a desiccator at ambient temperature, following a method adapted from the literature [6]. After 30 days of storage, the samples were analyzed using TGA as previously described. The percentage of fragrance retention (%RT) was calculated using Equation (4):

$$\%\mathrm{RT} = \frac{\%LE_{30}}{\%LE_0} \times 100 \qquad (4)$$

where $\%LE_{30}$ is the loading efficiency after 30 days of storage and $\%LE_0$ is the initial loading efficiency.

3 Results and discussion

3.1 UV-vis spectra of fragrance compounds

Three fragrance molecules were investigated in this study: D-limonene (DL), benzyl acetate (BA), and geraniol (GE), as shown in Fig. 1. Geraniol is a terpene alcohol known for its characteristic rose-like scent. The UV–vis absorption spectra of the fragrance compounds are presented in figure 2. Both DL and GE exhibited maximum absorbance (λ_{max}) around 203 nm, while BA showed a λ_{max} at 207 nm, which aligns closely with previously reported values [16-18].

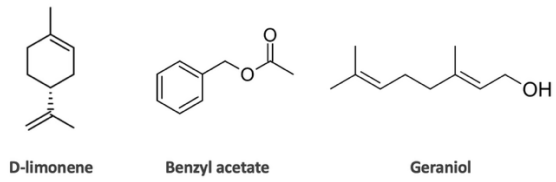

Fig. 1. Molecular structure of fragrance molecules used in this works.

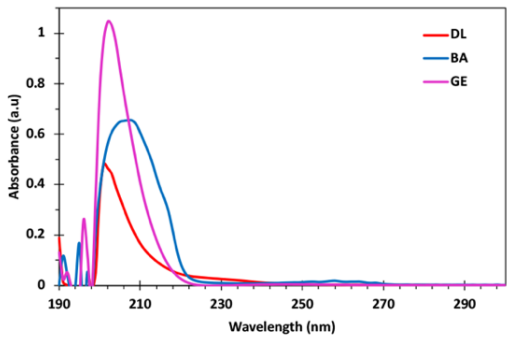

Fig. 2. UV-vis spectra of fragrance compounds.

3.2 SEM and N_2 adsorption-desorption analyses of zeolite

Zeolites are typically porous materials with a microporous structure, resulting in a high surface area that is suitable for adsorption applications. Their narrow pore distribution also enables controlled fragrance release. In this study, the morphology of the natural zeolite was examined using SEM, as shown in Figure 3(a). The SEM image reveals that the zeolite particles form aggregates with a highly rough surface, suggesting the presence of significant porosity.

To further confirm the porosity, N_2 adsorption–desorption analysis was performed to determine the specific surface area, pore size, and pore volume. As shown in Figure 3(b), the isotherm corresponds to type IV according to the IUPAC classification, indicating a mesoporous structure with pore sizes in the range of 2–50 nm [19]. The zeolite exhibited a specific surface area of 98.209 m^2/g, an average pore size of 10.9 nm, and a pore volume of 0.4852 cm^3/g. The relatively low surface area and large pore size are consistent with previous reports on natural zeolites [20-22].

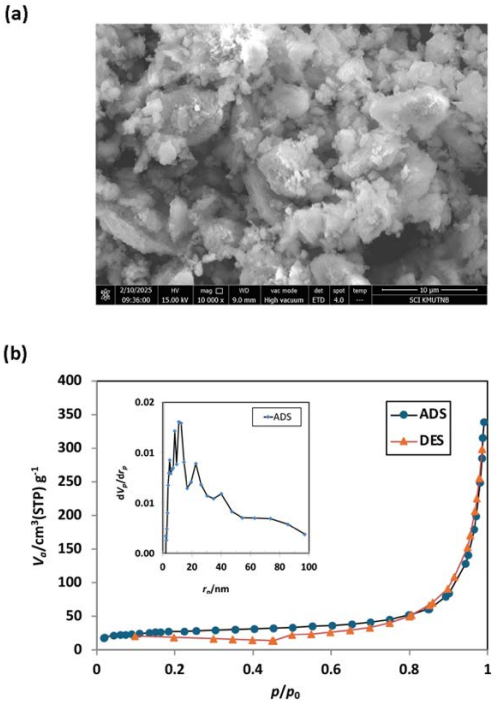

Fig. 3. (a) SEM image of zeolite at 10,000× magnification and (b) N_2 adsorption–desorption isotherm and pore size distribution curve.

3.3 X-ray diffraction

X-ray diffraction (XRD) analysis was conducted to investigate the crystalline structure of the natural zeolite. As illustrated in Fig. 4, the diffraction pattern was recorded over a 2θ range of 1° to 80°. The presence of sharp and well-defined peaks in the XRD pattern confirms the crystalline nature of the zeolite. The observed diffraction peaks correspond to the crystalline phase of clinoptilolite ($(K_2,Na_2,Ca)_3[Al_6Si_{30}O_{72}]\cdot 20H_2O$, IUPAC code: HEU), with characteristic peaks at 2θ values of 9.78°, 11.16°, 22.40°, and 29.92° [22, 23], as well as the crystalline phase of quartz, identified by a prominent peak at 2θ of 26.62° [21].

After fragrance loading (DL/Ze, BA/Ze, and GE/Ze), the XRD patterns and peak intensities remained largely unchanged compared to those of the natural zeolite, indicating that the loading process did not affect the

crystalline structure of the zeolite. However, co-loading with Tween 80 (GE-Tw/Ze) showed a noticeable reduction in peak intensity, suggesting partial disruption of the crystal structure during the encapsulation process. Nonetheless, the overall structural stability of the zeolite was largely preserved following fragrance incorporation.

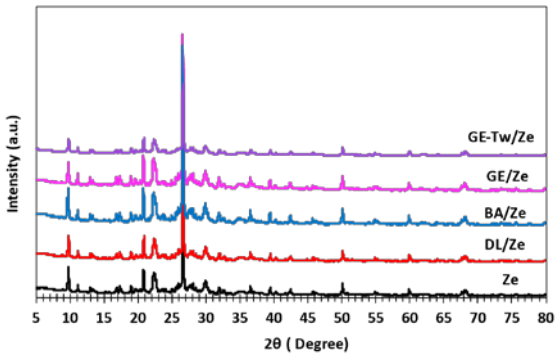

Fig. 4. XRD diffractograms of zeolite, fragrance-loaded zeolites, and geraniol-loaded zeolite with Tween 80.

3.4 Color analysis

The total color difference (ΔE) between the fragrance-loaded zeolite and natural zeolite was evaluated to assess the visual changes resulting from fragrance encapsulation, which is important for the quality control of commercial products, as such changes may affect the final appearance of the end products. The CIELAB color parameters of the zeolite samples are summarized in Table 1.

Table 1. Color of zeolite and fragrance-loaded zeolites with and without T80.

Sample	L*	a*	b*	ΔE
Ze	78.07 ± 0.02	5.23 ± 0.00	13.36 ± 0.01	-
DL/Ze	76.95 ± 0.01	5.10 ± 0.01	13.03 ± 0.01	1.16
BA/Ze	70.31 ± 0.01	5.79 ± 0.01	13.16 ± 0.01	7.79
GE/Ze	64.60 ± 0.00	7.78 ± 0.01	17.63 ± 0.01	14.36
DL-Tw/Ze	65.71 ± 0.01	7.92 ± 0.01	18.19 ± 0.10	14.23
BA-Tw/Ze	64.64 ± 0.01	8.62 ± 0.00	19.08 ± 0.00	15.05
GE-Tw/Ze	66.70 ± 0.00	7.92 ± 0.01	18.19 ± 0.10	12.72

In general, untrained human eyes can perceive color differences when ΔE exceeds 2. The greater the ΔE value, the more noticeable the difference to the human eye [24, 25].

Natural zeolite exhibited a high L* value along with positive a* and b* values, indicating a bright color with reddish and yellowish tones. After fragrance loading, noticeable changes in the color parameters were observed. The L* value tended to decrease, indicating a darker shade, while the a* and b* values increased, suggesting enhanced red and yellow components.

Among the tested fragrances, GE induced the most pronounced color change. The presence of T80 appeared to enhance this effect, which may be attributed to their larger molecular size and their interaction with the zeolite surface, potentially influencing surface properties and light reflection behavior.

3.5 FTIR

Figure 5. FT-IR spectra comparing (a) pure zeolite and individual fragrance molecules, (b) fragrance-loaded zeolite without T80, and (c) fragrance-loaded zeolite with T80.

FTIR spectrum of zeolite (Figure 5(a)) exhibits characteristic bands corresponding to Si–O(Si) and Si–O(Al) vibrations in the range of 1200–400 cm^{-1}. Additionally, absorption bands around 1600 cm^{-1} and 3700 cm^{-1} are attributed to H–O bending and stretching vibrations, respectively, indicating the presence of adsorbed water molecules within the zeolite structure [26].

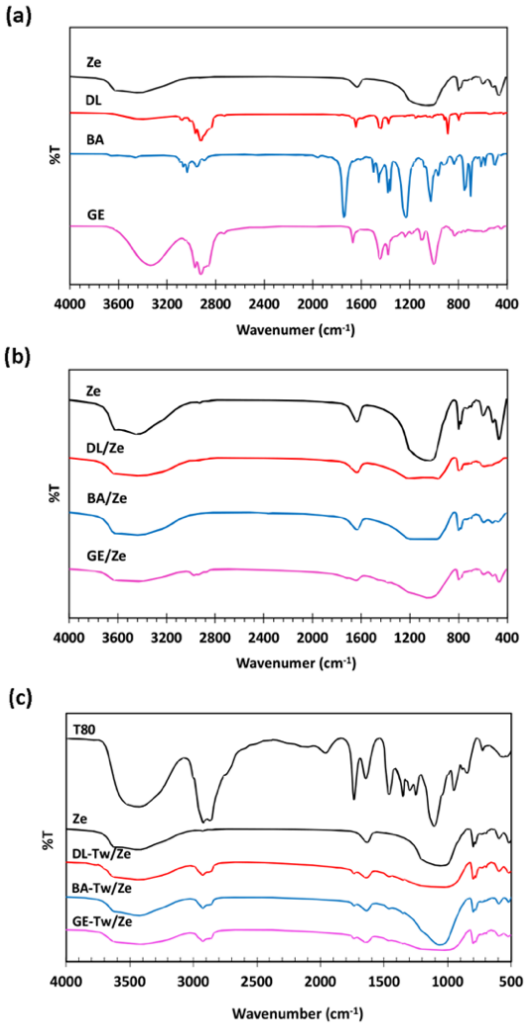

Fig. 5. FTIR spectra of (a) zeolite and fragrance compounds, (b) fragrance-loaded zeolites, and (c) fragrance-loaded zeolite with T80.

For D-limonene, the spectrum displays distinct peaks at 2975 cm^{-1} and 2920 cm^{-1}, assigned to C–H stretching

vibrations of methyl groups (–CH_3). The C=C stretching vibrations of both cycloalkene and disubstituted alkene structures are observed at 1645 cm^{-1}. CH_2 scissoring vibrations appear at 1452 cm^{-1} and 1376 cm^{-1}, while the =C–H out-of-plane bending of a terminal methylene group is noted at 887 cm^{-1} [27].

The FTIR spectrum of BA shows characteristic aromatic C–H stretching at 3035 cm^{-1}, a strong ester C=O stretching band at 1742 cm^{-1}, and C–O stretching of the ester group at 1229 cm^{-1}. Additionally, C–H out-of-plane bending vibrations of the aromatic ring are observed at 750 cm^{-1} and 698 cm^{-1}.

GE exhibits a broad O–H stretching band of the alcohol group at 3334 cm^{-1}. The C–H stretching vibrations of methyl groups (–CH_3) are observed at 2968 cm^{-1} and 2918 cm^{-1}. A prominent C=C stretching vibration of the alkene group appears at 1669 cm^{-1}, while the C–O stretching vibration of the alcohol functional group is detected at 1001 cm^{-1} [28].

Fragrance-loaded zeolite samples (DL/Ze, BA/Ze, and GE/Ze) (Figure 5 (b)) showed the major characteristic bands of the zeolite. However, distinct peaks corresponding to the fragrance molecules were generally not clearly observed, except in the GE/Ze sample, which showed peaks around 2976 cm^{-1} and 2939 cm^{-1}, corresponding to the C–H stretching of methyl groups (–CH_3), confirming the presence of geraniol. The absence of distinct fragrance peaks in the other sample maybe attributed to the low fragrance-to-zeolite ratio. Moreover, during the encapsulation process, fragrances with higher boiling points—such as geraniol—are more likely to remain entrapped within the zeolite matrix, resulting in higher residual content post-encapsulation.

In addition, the sample containing T80 (Figure 5(c)) exhibits weak signals of characteristic vibration bands corresponding to C–H stretching of hydrocarbon chains at 2925 cm^{-1} and C=O stretching of the ester group at 1737 cm^{-1}, confirming the presence of T80 after encapsulation [10].

3.6 Fragrance loading and encapsulation efficiencies

The fragrance loading efficiency (%LE) and encapsulation efficiency (%EE) were estimated and are presented in Fig. 6. As observed, the encapsulation systems containing T80 exhibited more consistent %LE and %EE values compared to systems without T80. In the presence of T80, the %LE of DL-Tw/Ze, BA-Tw/Ze, and GE-Tw/Ze ranged narrowly between 15–17%, while the %EE values were between 23–28%. In contrast, systems without T80 (DL/Ze, BA/Ze, and GE/Ze) showed substantial variation in both %LE (8-30%) and %EE (11-42%). These findings suggest that the presence of T80 contributes to improved consistency in the encapsulation of different fragrance molecules. However, additional analytical techniques such as TGA–MS or gas chromatography are recommended to confirm these results.

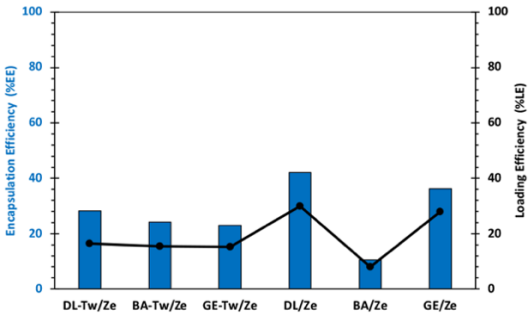

Fig. 6. Encapsulation efficiency (%EE, bar graph) and loading efficiency (%LE, line graph) of fragrance-loaded zeolite with and without the addition of T80.

3.7 Fragrance retention

To evaluate fragrance retention, the encapsulated samples were stored in a desiccator at ambient temperature for 30 days, after which the remaining fragrance content in the carriers was measured. As shown in figure 7, D-limonene—having the lowest molecular weight (136.23 g/mol) and boiling point (176°C)—exhibited the lowest retention. In contrast, geraniol, with the highest molecular weight (154.25 g/mol) and boiling point (230°C) among the tested compounds, showed the highest retention. Notably, the presence of T80 enhanced fragrance retention, particularly for low molecular weight and more volatile compounds such as D-limonene and benzyl acetate (150.18 g/mol, 134°C). The hydrophilic head of T80 can interact with the zeolite surface via hydrogen bonding, while its hydrophobic tail interacts with fragrance molecules through London dispersion forces. This dual interaction mechanism helps prolong the release of fragrance compounds. These findings highlight the significant role of T80 as a fragrance retention enhancer, suggesting its potential application in industrial formulations requiring prolonged aroma release.

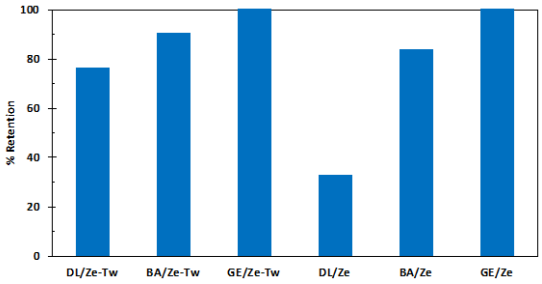

Fig. 7. Fragrance retention after storage at ambient temperature for 30 days.

4 Conclusion

This study highlights the effectiveness of natural zeolite as a carrier for fragrance encapsulation, particularly when modified with Tween 80 (T80). The incorporation of T80, a non-ionic surfactant, improved the uniformity of loading and encapsulation efficiency across structurally diverse fragrance molecules. Zeolite facilitated the entrapment and stabilization of fragrance molecules, while T80 improved molecular dispersion and retention,

particularly for low molecular weight (small molecules) and volatile compounds such as D-limonene and benzyl acetate. The results underscore the synergistic role of zeolite and T80 in modulating encapsulation behavior and long-term fragrance retention, offering a promising approach for the development of advanced delivery systems with sustained aroma release for industrial applications.

This research was funded by Faculty of Applied Science, King Mongkut's University of Technology North Bangkok, Contract No. 680036. We gratefully acknowledge the Department of Industrial Chemistry, Faculty of Applied Science, King Mongkut's University of Technology North Bangkok, and the Department of Chemical Engineering, Faculty of Engineering, Mahidol University, for their valuable support and provision of essential analytical instruments.

Author contributions

Natnicha Kongyang.: Investigation and Methodology. **Sukanya Sudmee.**: Investigation and Methodology. **Rapeeporn Wannarat.**: Investigation and Methodology. **Sukanya Thepwatee.**: Conceptualization, Data Curation, Formal Analysis, Graphic Preparation, Writing – Original Draft, Reviewing, and Editing, Funding Acquisition, Supervision, Project Administration, and Validation.

References

1. R. S. Herz, M. Larsson, R. Trujillo, M. C. Casola, F. K. Ahmed, S. Lipe, M. E. Brashear, A three-factor benefits framework for understanding consumer preference for scented household products: psychological interactions and implications for future development. Cogn. Res.: Princ. Implic. **7**, 28 (2022). https://doi.org/10.1186/s41235-022-00378-6
2. R. K R, S. Gopi, P. Balakrishnan, Introduction to Flavor and Fragrance in Food Processing. Flavors and Fragrances in Food Processing: Preparation and Characterization Methods (American Chemical Society, 2022). http://doi.org/10.1021/bk-2022-1433.ch001
3. E. Guzmán, A. Lucia, Essential Oils and Their Individual Components in Cosmetic Products. Cosmetics. **8**, 114 (2021). https://doi.org/10.3390/cosmetics8040114
4. S. P. Costa, O. S. Soares, C. A. Aguiar, I. C. Neves, Fragrance carriers obtained by encapsulation of volatile aromas into zeolite structures. Ind. Crops Prod. **187**, 115397 (2022). https://doi.org/10.1016/j.indcrop.2022. 115397
5. K. Ayuningtyas, E. Kusrini, W.W. Prihandini, Development of fragrance carrier from Luffa acutangula using zeolite A. IOP Conf. Ser.: Mater. Sci. Eng. **1098**, 022005 (2021). https://doi.org/ 10.1088/1757899X/1098/ 2/ 022005
6. Z. Li, J. Huang, L. Ye, Y. Lv, Z. Zhou, Y. Shen, Y. He, L. Jiang, Encapsulation of highly volatile fragrances in Y zeolites for sustained release: Experimental and theoretical studies. ACS omega. **5**, 31925-31935 (2020). https:// doi.org/ 10.1021/acsomega.0c04822
7. S. Wang, D. Jiang, Z. Zhou, Y. Shen, L. Jiang, A novel photothermo-responsive nanocarrier for the controlled release of low-volatile fragrances. RSC Advances. **10**, 14867-14876 (2020) https://doi.org/10.1039/C9RA106 62F
8. Y. Tian, C. Lianghong, W. Zhang, Influence of Ionic Surfactants on the Properties of Nanoemulsions Emulsified by Nonionic Surfactants Span 80/Tween 80. J. Disper. Sci. Technol. **37**, 1511-1517 (2016). https:// doi.org/10.1080/01932691.2015.1048806
9. R. Wang, C. Ma, H. Yan, H. Zhao, P. Wang, S. Zhang, J. Ju, S. Yu, Z. Yin, Lecithin/Cholesterol/Tween 80 Liposomes for Co-Encapsulation of Vitamin C and Xanthoxylin. ACS Appl. Nano Mater. **7**, 5982-5995 (2024). https://doi.org/ 10.1021/acsanm.3c05884
10. F. Kerdmuanglek, T. Chomtong, S. Boonsith, T. Chutimasakul, J. Iemsam-arng, S. Thepwatee, Non-ionic surfactant-assisted controlled release of oxyresveratrol on dendritic fibrous silica for topical applications. J. Colloid Interface Sci. **646**, 342-353 (2023). https://doi.org/ 10.1016/j.jcis.2023.05.050
11. A. Kliszcz, A. Danel, J. Puła, B. Barabasz-Krasny, K. Możdżeń, Fleeting Beauty—The World of Plant Fragrances and Their Application. Molecules **26,** 2473 (2021). https://doi.org/10.3390/molecules26092473
12. P. Anandakumar, S. Kamaraj, M.K. Vanitha, D-limonene: A multifunctional compound with potent therapeutic effects. J. Food Biochem. **45,** e13566 (2021). https://doi.org/10.1111/jfbc.13566
13. W. Chen, A.M. Viljoen, Geraniol – A review update. S. Afr. J. Bot. **150**, 1205-1219 (2022). https://doi.org/ 10.1016/j.sajb.2022.09.012
14. G. Ye, Y. Sun, Z. Guo, K. Zhu, H. Liu, X. Zhou, M.O. Coppens, Effects of zeolite particle size and internal grain boundaries on Pt/Beta catalyzed isomerization of n-pentane. J. Catal. **360**, 152-159 (2018) https://doi.org/ 10.1016/j.jcat.2018.01.033
15. D. Tsivas, A. Vlyssides, A. Vlysidis, Monitoring of a III-Phase Olive Pomace Composting Process Using the CIELAB Colorimetric Method. Waste Biomass Valori. **12**, 5029-5039 (2021). https://doi.org/10.1007/s12649-021-01363-8
16. X. Feng, K. Feng, Q. Zheng, W. Tan, W. Zhong, C. Liao, Y. Liu, S. Li, W. Hu, Preparation and characterization of geraniol nanoemulsions and its antibacterial activity. Front. microbiol. **13**, (2022). https://doi.org/10.3389/fmicb.2022.1080300
17. B.R. Belem, G.V. Carapeto, M.G. Issa, H.G. Ferraz, Microemulsions: An Encapsulation Strategy to Increase the Thermal Stability of D-limonene. Pharmaceutics. **15**, 2564 (2023). https://doi.org/10.3390/ pharmaceutics15112564
18. D. McGinty, D. Vitale, C. S. Letizia, A. M. Api, Fragrance material review on benzyl acetate. Food Chem. Toxicol. **50**, S363-S84 (2012). https://doi.org/10.1016/ j.fct.2012.02.057
19. M. Thommes, K. Kaneko, A.V. Neimark, J. P. Olivier, F. Rodriguez-Reinoso, J. Rouquerol, S. S.W. Kenneth, Physisorption of gases, with special reference to the evaluation of surface area and pore

size distribution (IUPAC Technical Report). Pure Appl. Chem. **87**, 1051-1069 (2015). https://doi.org/10.1515/pac-2014-1117
20. A. Mockovčiaková, M. Matik, Z. Orolínová, P. Hudec, E. Kmecová, Structural characteristics of modified natural zeolite. J. Porous Mater. **15**, 559-564 (2008). https://doi.org/10.1007/s10934-007-9133-3
21. M. Silva, A. Lecus, Y. Lin, J. Corrao, Tailoring natural zeolites by acid treatments. J. Mater. Sci. Chem. Eng. **7**, 26-37 (2019). https://doi.org/10.4236/msce.2019.72003
22. M. Dosa, N. Grifasi, C. Galletti, D. Fino, M. Piumetti, Natural Zeolite Clinoptilolite Application in Wastewater Treatment: Methylene Blue, Zinc and Cadmium Abatement Tests and Kinetic Studies. Materials **15**, 8191 (2022). https://doi.org/10.3390/ma15228191
23. R. Malekian, J. Abedi-Koupai, S. S. Eslamian, Influences of clinoptilolite and surfactant-modified clinoptilolite zeolite on nitrate leaching and plant growth. J. Hazard. Mater. **185**, 970-976 (2011). https://doi.org/ 10.1016/ j.jhazmat.2010.09.114
24. O. E. Pecho, R. Ghinea, R. Alessandretti, M. M. Pérez, A. Della Bona, Visual and instrumental shade matching using CIELAB and CIEDE2000 color difference formulas. Dent. Mater. **32**, 82-92 (2016). https://doi.org/10.1016/j.dental.2015.10.015
25. T. U. Klinke, W. B. Hannak, K. Böning, H. A. Jakstat, E. Prause, Visual Tooth Color Determination with Different Reference Scales as an Exercise in Dental Students' Education. Dent. J. **11**, 275 (2023). https://doi.org/ 10.3390/dj11120275
26. O. Korkuna, R. Leboda, J. Skubiszewska-Zie¸ba, T. Vrublevs'ka, V. M. Gun'ko, J. Ryczkowski, Structural and physicochemical properties of natural zeolites: clinoptilolite and mordenite. Microporous Mesoporous Mater. **87**, 243-254 (2006). https://doi.org/10.1016/ j.micromeso.2005.08.002
27. I. H. Arachchilage, M. K. Patel, J. Basi, J. P. Harmon, Environmentally Friendly Radiation Hard d-Limonene and Laccol Copolymers Synthesized via Cationic Copolymerization. Polym. Eng. Sci. **60**, 607-618 (2020). https://doi.org/10.1002/pen.25319
28. K. N. Rosalina, T. Wukirsari, S. Handayani, S. Hudiyono, Utilization of Silica Gel for the Synthesis of Geranyl Laurate and Citronellyl Laurate. Bull. Chem. React. Eng. Catal. **19**, 350-360 (2024). https://doi.org/ 10.9767/bcrec.20159